Macromolecules

ARTICLE

pubs.acs.org/Macromolecules

Phase Behavior of Binary Blends of Block Copolymers Having Hydrogen Bonding

Sung Hyun Han and Jin Kon Kim*

National Creative Research Initiative Center for Block Copolymer Self-Assembly, Department of Chemical Engineering, Pohang University of Science and Technology, Pohang, Kyungbuk 790-784, Republic of Korea

Victor Pryamitsyn and Venkat Ganesan*

Department of Chemical Engineering, University of Texas at Austin, Austin, Texas 78712, United States

Supporting Information

ABSTRACT: Phase behavior of binary blends consisting of high molecular weight polystyrene-*block*-poly(2-vinylpyridine) copolymer (PS-*b*-P2VP) and low molecular weight polystyrene-*block*-poly(4-hydroxystyrene) copolymer (PS-*b*-PHS) was investigated by using small-angle X-ray scattering and transmission electron microscopy. Both PS-*b*-P2VP and PS-*b*-PHS exhibited lamellar microdomain over the entire experimental temperatures up to 300 °C. When the weight fraction of PS-*b*-PHS in the blend was less than 0.1, the lamellar microdomains were maintained. However, with increasing amount of PS-*b*-PHS, the microdomains in the blends were transformed to hexagonally packed (HEX) cylindrical microdomains and body-centered cubic (BCC) spherical microdomains. On the other hand, when a relatively high molecular weight of PS-*b*-PHS was used, the BCC spherical microdomains were not observed even at a large weight fraction of PS-*b*-PHS in the blend, but HEX cylindrical microdomains were formed. The phase behaviors observed experimentally were rationalized by the results of the self-consistent mean-field theory. Based on the theoretical results, some of the PS-*b*-PHS dissolves into P2VP microdomains and thereby increases the effective volume of P2VP/PHS phase because of hydrogen bonding between P2VP and PHS blocks. In the case of smaller molecular weight of PS-*b*-PHS, the dissolved amount is significant because the favorable interactions of P2VP/PHS chains becomes dominant over the relatively small enthalpic penalty between PS/P2VP in the P2VP microdomains as well as the gain of the translational entropy of the PS-*b*-PHS chains. The increase in the effective volume of the PHS/P2VP phase leads to a transformation of the microdomains in the blends from lamellar to HEX cylindrical microdomains and BCC spherical microdomains. On the other hand, when a relatively higher molecular weight of PS-*b*-PHS was used, the effective volume of the P2VP/PHS phase was not increased greatly because of a large enthalpic loss arising from the contact between PS/P2VP as well as a small gain in the translational entropy. Consequently, only lamellar and HEX cylindrical microdomains are observed.

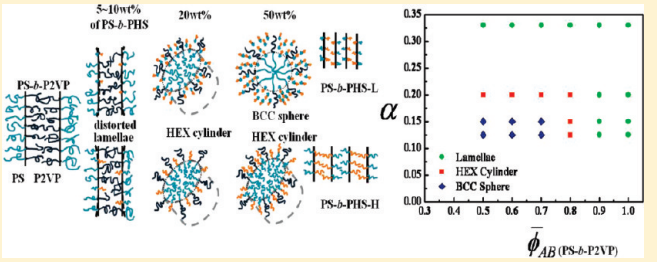

1. INTRODUCTION

Block copolymers have been extensively investigated because of their self-organization nature into many periodic nanoscale structures.[1−20] To control nanostructures, many research groups have employed binary blends of two block copolymers.[21−40] Hashimoto and co-workers[29−32] studied phase behavior of binary blends consisting of a long asymmetric polystyrene-*block*-polyisoprene copolymer (PS-*b*-PI) with body-centered cubic (BCC) spherical microdomains and short symmetric PS-*b*-PIs. They showed that the morphology of binary blends was transformed from BCC spheres to lamellar microdomains with increasing amount of a short block copolymer. One interesting observation of the binary blends of two lamellar forming PS-*b*-PIs with different molecular weights is that the morphology of binary blends was transformed from the lamellae to hexagonally packed (HEX) cylinderical microdomains, despite the fact that both neat block copolymers showed lamellar microdomains.[33,34] This unusual behavior is due to a slight asymmetry of a short PS-*b*-PI, which increases the curvature of the lamellar microdomains.

Kimishima et al.[35] studied the microdomain structures in binary blends between PS-*b*-poly(ethylenepropylene) copolymer (PS-*b*-PEP) and PS-*b*-(partially hydrogenated polyisoprene) copolymer (PS-*b*-HPI) depending on the degree of hydrogenation for HPI block. They showed that with increasing the repulsive interaction between PEP and HPI blocks, which depends on the degree of hydrogenation for HPI blocks, macrophase separation occurred. Han and co-workers[36] reported phase diagrams for binary blends consisting of PS-*b*-PI and PS-*b*-polybutadiene copolymer

Received: March 31, 2011
Revised: May 12, 2011
Published: June 03, 2011

(PS-*b*-PB) with various molecular weights and volume fractions. The order-to-disorder transition temperature (T_{ODT}) of the blends of highly asymmetric block copolymers showed a positive deviation from linearity, while that for blends of nearly symmetric block copolymers exhibited an almost linear relationship. Hillmyer and co-workers[37] studied the morphology of PS-*b*-polylactide copolymer (PS-*b*-PLA)/PS-*b*-poly(ethylene oxide) copolymer (PS-*b*-PEO) blends. The PLA and PEO blocks in these blends were miscible, and the crystallinity of PEO block was significantly reduced due to its confinement induced by the PS matrix.

On the other hand, some research groups[38−40] investigated the phase behavior of binary blends of the block copolymers that the hydrogen bonding could be formed between block components. Matsushita and co-workers[38,39] observed many new morphologies of binary blend of PI-*b*-poly(2-vinylpyridine) copolymer (P2VP) and PS-*b*-poly(4-hydroxystyrene) copolymer (PHS) where the hydrogen bond could be formed between P2VP and PHS. Kuo and co-workers[40] investigated the phase transformation of mixtures of PS-*b*-PHS and various homopolymers of poly(4-vinylpyridine) (P4VP), poly(methyl methacrylate) (PMMA), and PHS. Interestingly, only PS-*b*-PHS/P4VP mixture showed phase transformations from lamellae, gyroid, HEX cylinders, and finally to BCC spherical microdomains. This is because a strong hydrogen bond exists between PHS and P4VP.

It is generally not easy to obtain HEX cylinders or BCC spheres for binary blends of two nearly symmetric block copolymers having the same chemical structure. However, it would be possible for the binary blends with two nearly symmetric block copolymers having different chemical structures, where an intermolecular interaction such as hydrogen bonding exists. To test this postulation, we employed the binary blends of PS-*b*-P2VP and PS-*b*-PHS, where the hydrogen bond is expected between P2VP and PHS chain. Then, we investigated the phase behavior on binary blends by using small-angle X-ray scattering (SAXS) and transmission electron microscopy (TEM). Both neat PS-*b*-P2VP and PS-*b*-PHS showed lamellar microdomains over the entire experimental temperature. We found that with increasing weight fraction of lower molecular weight PS-*b*-PHS the lamellar microdomains were transformed to HEX cylinders and BCC spheres. On the other hand, when a relatively higher molecular weight PS-*b*-PHS was used, the BCC spheres were not observed even at large amount of PS-*b*-PHS in the blend. The phase behaviors observed experimentally were explained by the self-consistent mean-field theory.[41−46]

Table 1. Molecular Characteristics of Symmetric PS-*b*-P2VP and PS-*b*-PHS

sample code	M_w	M_w/M_n	f_{PS}[c]
PS-*b*-P2VP	114 000	1.08	0.5
PS-*b*-PHS-L	8 000[a]	1.08[b]	0.53
PS-*b*-PHS-H	57 400[a]	1.07[b]	0.49

[a] Calculated by M_n of PS precursor measured by GPC using PS standards and the weight fraction of PS in PS-*b*-PHS measured by ^{1}H NMR. [b] M_w/M_n of PS-*b*-P*t*BS measured by GPC using PS standards. [c] Calculated by ^{1}H NMR and known density at room temperature (PS = 1.05 g/cm^3; P2VP = 1.15 g/cm^3; PHS = 1.16 g/cm^3).

2. EXPERIMENTAL SECTION

A high molecular weight PS-*b*-P2VP was purchased from Polymer Source. PS-*b*-PHSs with two different molecular weights were prepared via the hydrolysis reaction of PS-*b*-poly(4-*tert*-butoxystyrene) copolymers (PS-*b*-P*t*BOS)s,[47] which were synthesized by the anionic polymerization of styrene and 4-*tert*-butoxystyrene monomers in tetrahydrofuran (THF) at −78 °C under an argon environment using *sec*-butyllithium (*s*-BuLi) as an initiator. All the weight- and number-average molecular weights were measured by size exclusion chromatography using PS standards in THF solution, and the volume fraction of PS (f_{PS}) was determined by ^{1}H nuclear magnetic resonance spectroscopy. The molecular characteristics of block copolymers used in this study are summarized in Table 1.

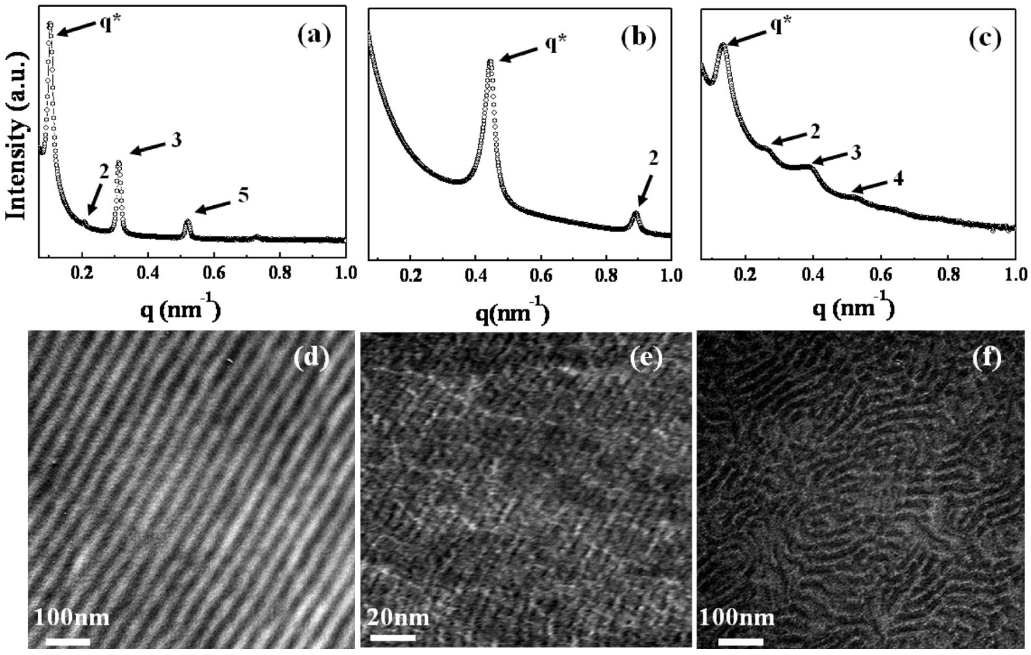

Figure 1. SAXS profiles (upper panels) and TEM images (lower panels) for neat PS-*b*-P2VP (a, d), PS-*b*-PHS-L (b, e), and PS-*b*-PHS-H (c, f).

dx.doi.org/10.1021/ma200747d |*Macromolecules* 2011, 44, 4970–4976

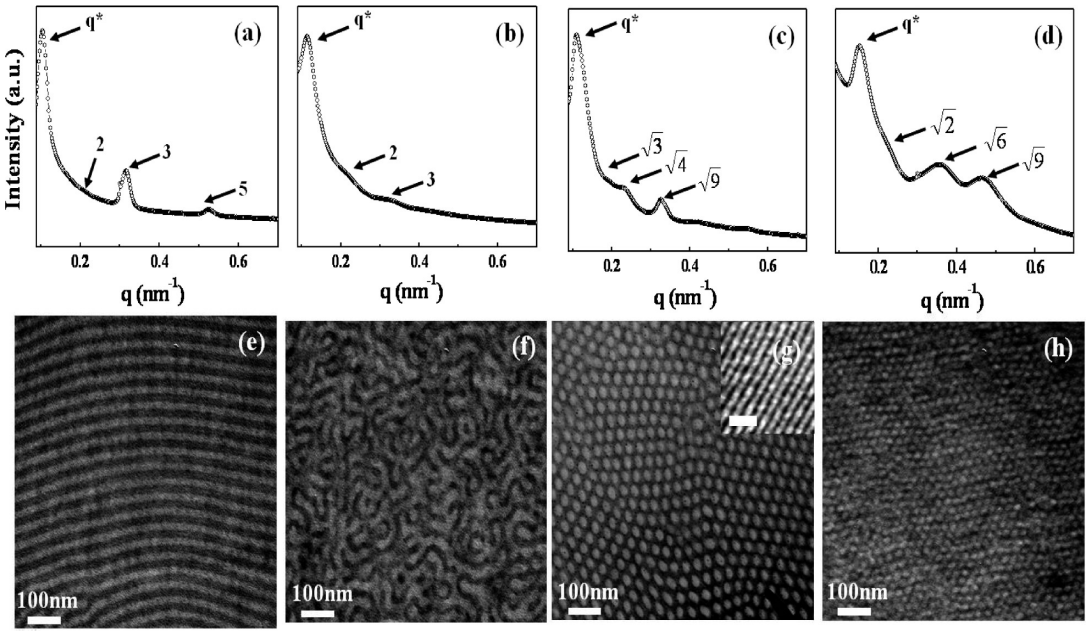

Figure 2. SAXS profiles and TEM images of PS-*b*-P2VP/PS-*b*-PHS-L blend with various compositions. The weight fraction of PS-*b*-PHS-L in the blend: 0.05 (a, e), 0.1 (b, f), 0.2 (c, g), and 0.5 (d, h). Inset in (g) is TEM image (scale bar = 100 nm) of the sample cut along the cylinder axis.

All the binary blends with various compositions of PS-*b*-P2VP and PS-*b*-PHSs were prepared via solution casting using dimethylformamide solvent, followed by a slow solvent evaporation at 100 °C, and a thermal annealing at 180 °C for 5 days under vacuum, followed by quenched to room temperature.

SAXS measurements were performed at room temperature on beamline 4C1 at the Pohang Light Source (Korea), where a W/B4C double multilayer delivered monochromatic X-rays on the samples with a wavelength of 0.1608 nm and a sample-to-detector distance of 2 m.[48] A 2-D CCD camera (Princeton Instruments, SCX-TE/CCD-1242) was used to collect the scattered X-rays. Microdomains for binary blends were directly observed using TEM (Hitachi 7600) operating at 100 kV. The specimens were stained with iodine for 2 h at room temperature, which was selective to PHS or P2VP microdomains.

3. RESULTS AND DISCUSSION

Figure 1 gives SAXS profiles and TEM images for neat PS-*b*-P2VP, PS-*b*-PHS-L, and PS-*b*-PHS-H. All neat block copolymers exhibited lamellar microdomain, which is quite expected because all the block copolymers have nearly symmetric volume fractions (around 0.5). Interestingly, although the molecular weight of PS-*b*-PHS-L is quite low (8000), it exhibited lamellar microdomains over the entire range of experimental temperatures up to 300 °C (see Figure S1 in the Supporting Information). This is because the Flory−Huggins segmental interaction parameter (χ) between PS and PHS is very high (~0.68).[49]

Figure 2 shows SAXS profiles and TEM images of binary blends with four different blend compositions (95/5; 90/10; 80/20; and 50/50 w/w) of PS-*b*-P2VP and PS-*b*-PHS-L. The 95/5 (w/w) PS-*b*-P2VP/PS-*b*-PHS-L blend shows lamellar microdomains verified by SAXS profile (Figure 2a) and TEM image (Figure 2e). When the weight fraction of PS-*b*-PHS-L is increased to 0.1, the lamellar microdomains are still maintained, as shown in the SAXS profile (Figure 2b). However, the ordering of the lamellar microdomains becomes poor compared with that of 95/5 (w/w) PS-*b*-P2VP/PS-*b*-PHS-L blend (compare Figure 2f vs Figure 2e). As the amount of PS-*b*-PHS in the blend increases to 20 wt %, the blend shows HEX cylindrical microdomains because the SAXS peaks are located at positions of $1:\sqrt{3}:\sqrt{4}:\sqrt{9}$ (Figure 2c) and TEM image (Figure 2g). When the amount of PS-*b*-PHS in the blend is further increased to 50 wt %, the blend shows BCC spherical microdomains, as demonstrated by the SAXS profile (Figure 2d) which shows the peaks at positions of $1:\sqrt{2}:\sqrt{6}:\sqrt{9}$ as well as TEM image (Figure 2h).

Previously, Hashimoto and co-workers[33] reported that HEX cylindrical microdomains were formed by blending of two lamellar forming PS-*b*-PIs with different molecular weights. However, in this situation, the phase transformation from lamellar to HEX cylindrical microdomains was ascribed to a slight asymmetry of a short PS-*b*-PI where the volume fraction of PS is 0.40! Also, they could not observe spherical microdomains for the above blend. Considering this fact, we consider that the phase transformation of PS-*b*-P2VP/PS-*b*-PHS-L blend is ascribed to the increased effective volume of P2VP phase due to the hydrogen bonding between P2VP and PHS blocks. We found that the degree of the hydrogen bonding between P2VP and PHS increases with increased amount of PS-*b*-PHS-L in the blend, confirmed by Fourier transform infrared spectroscopy (Figure S2 in the Supporting Information).

We also prepared another binary blend using PS-*b*-PHS with a relatively large molecular weight (PS-*b*-PHS-H). Figure 3 gives the SAXS profiles and the TEM images of binary blends with two different blend compositions. When the content of PS-*b*-PHS-H in the blend is 20 wt %, the SAXS profile and TEM image show that lamellar morphologies are changed to the HEX cylindrical microdomains (Figures 3a,c). But, the phase transformation into the BCC spherical microdomains did not happen even when the weight fraction PS-*b*-PHS-H was increased to 0.5 (Figures 3b,d). Here, we do not observe any macrophase separation between two block copolymers in this blend verified by SAXS and TEM. On the other hand, 50/50 (w/w) PS-*b*-P2VP/PS-*b*-PHS-L blend showed

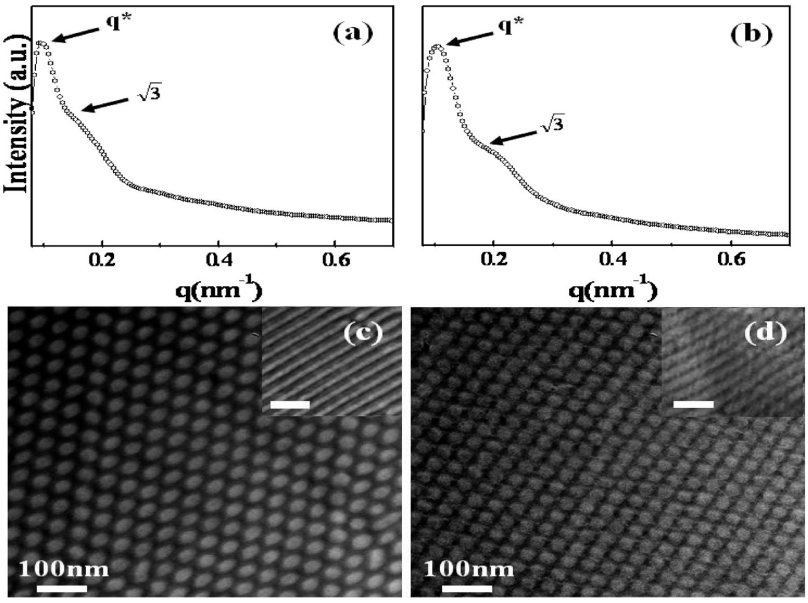

Figure 3. SAXS profiles and TEM images of 80:20 w/w (a, c) and 50:50 w/w (b, d) PS-*b*-P2VP/PS-*b*-PHS-H blends. Insets in (c) and (d) are TEM images (scale bar = 100 nm) of the samples cut along the cylinder axis.

BCC spherical microdomains, as confirmed with the SAXS profile and TEM image in Figures 2d,h.

4. DISCUSSION AND SELF-CONSISTENT FIELD THEORY RESULTS

To glean insights into the mechanisms underlying the experimental results, we performed self-consistent field theory (SCFT) calculations for the phase behavior of binary blends of AB (PS-*b*-P2VP) and AC diblock copolymers (PS-*b*-PHS). Since SCFT used in this study has been well-established in many literatures,[41−46] the details of the model are presented in the Supporting Information. The theory involves the following parameters: (i) $\chi_{AB}N_{AB}$, $\chi_{BC}N_{AB}$, and $\chi_{AC}N_{AB}$, which quantifies the segregation power. Here, χ_{ij} is the Flory−Huggins interaction parameter between i and j, and N_{AB} and N_{AC} are the total numbers of segments (or degree of polymerization) of AB and AC, respectively; (ii) $\bar{\phi}_{AB}$, the overall volume fraction of the AB in the blend; (iii) $\alpha = N_{AC}/N_{AB}$; and (iv) f_{AB} and f_{AC}, the volume fraction of A segments in the AB and AC.

Experimental conditions reported in this paper correspond to the strong-segregation regime, which poses numerical challenges in the implementation of SCFT. Since the objective was to glean insights into the experimental observations, we aimed for a qualitative comparison with the experimental observation rather than quantitative comparison. We chose representative values for the above parameters which mimic the experimental conditions: (i) $N_{AB} > N_{AC}$; (ii) $\chi_{AB}N_{AB} > 10.5$, $\chi_{AC}N_{AC} > 10.5$. This corresponds to the fact that the temperature is below T_{ODT} of both AB and AC; (iii) χ_{AC} is approximately 6−7 times the value of χ_{AB}.[49−52] Explicitly, we fixed $f_{AB} = f_{AC} = 0.5$, $\chi_{AB}N_{AB} = 20.0$, and $\chi_{AC}N_{AB} = 120$. Finally, we varied α between 1/8 and 1 to investigate the effect of molecular weights of AC and AB on the phase behavior, although we only report the results for $\alpha \leq 1/3$. A special mention is to be made about χ_{BC}, which is the Flory−Huggins parameter between P2VP and PHS. While there is known to be H-bonding interaction between P2VP and PHS,[53,54]

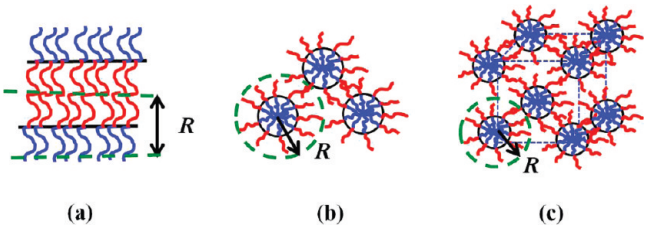

Figure 4. Unit cell representations for lamellar (a), cylindrical (b), and spherical (c) microdomains. R denotes the dimension of the unit cell over which the free energy is minimized.

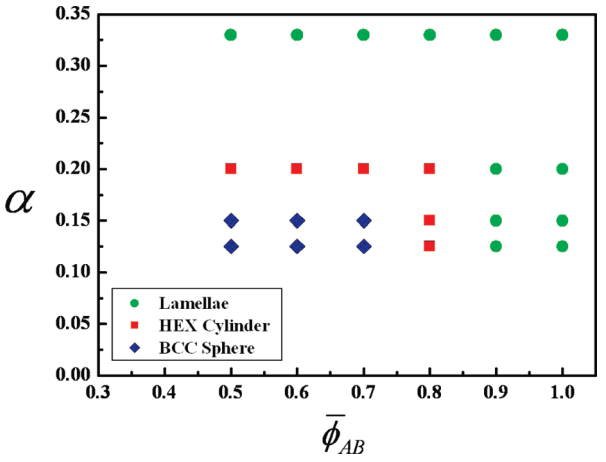

Figure 5. SCFT predictions of equilibrium morphology of AB/AC blend depending on α and $\bar{\phi}_{AB}$.

a realistic modeling of such interactions is not straightforward within a coarse-grained theory such as polymer SCFT. Consequently, we used a simple model wherein the favorable interaction between P2VP and PHS was modeled through $\chi_{BC} < 0$.[55] To

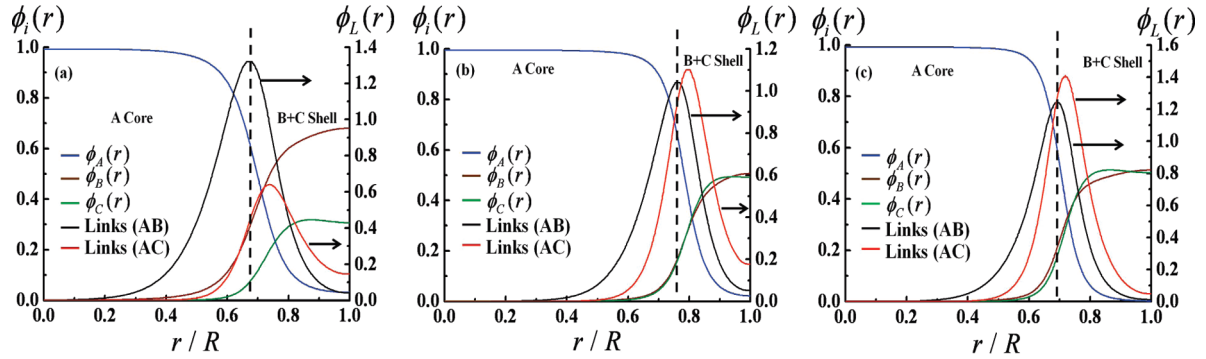

Figure 6. Local volume fractions of A, B, and C components, denoted $\phi_A(r)$, $\phi_B(r)$, and $\phi_C(r)$, respectively, as a function of the radial coordinate r normalized by the equilibrium size R of the unit cell. The core region consists of A segments and the corona/shell region consists mainly of B and C segments. The dashed line corresponding to the peak in the link distribution of AB represents an approximate demarcation between the core and the shell regions. Also shown are the number density distributions of the link segments of the AB and AC copolymers (normalized such that $\int_0^1 dr\, \phi_L(r) \propto \bar{\phi}_i$, where $\bar{\phi}_i = \bar{\phi}_{AB}$ or $\bar{\phi}_{AC}$): (a) $\alpha = 0.125$; $\bar{\phi}_{AB} = 0.8$ for which the equilibrium morphology is HEX cylindrical microdomains; (b) $\alpha = 0.125$; $\bar{\phi}_{AB} = 0.5$ for which the equilibrium morphology is BCC spherical microdomains; (c) $\alpha = 0.2$; $\bar{\phi}_{AB} = 0.5$ for which the equilibrium morphology is HEX cylindrical microdomains.

investigate the role of H-bonding interaction on the phase behavior, χ_{BC} is simply varied.

Numerical implementation of SCFT requires in general the solution of the equations arising in self-consistent theory in three-dimensional space with periodic boundary conditions. Because of the computational complexity of such a procedure in this work, we adopt a simpler, albeit approximate, methodology termed the "unit-cell" approach.[43−45] In this approach, the preferred morphology is determined by comparing the equilibrium free energies of candidate structures with the free energies themselves computed by using a unit cell of the same symmetry as the assumed structure. For instance, the free energy of the spherical morphology is computed by assuming a spherical cell with appropriate dimensions (over which the free energy is eventually minimized). In a similar manner, rectangular and cylindrical unit cells are used for computing the free energies of the lamellar and cylindrical morphologies, respectively. Thus, at any given stage, the equations are to be solved only in one-dimensional (rectangular or curvilinear) space, which leads to a substantial reduction in the computational time. Subsequently, the free energies of these morphologies themselves are compared to determine the "preferred" or equilibrium morphology for a given set of parameters. While this method is necessarily approximate in that it uses a unit cell of the morphology, prior calculations by Matsen in the context of diblock copolymers and their blends with homopolymers have suggested that the phase boundaries are quantitatively captured within this approximation.[43−45] The size of the equilibrium unit cell for the preferred morphology is denoted as R, as shown in Figure 4, for three microdomains (lamellae, HEX cylinders, and BCC spheres).

Figure 5 shows the predicted equilibrium morphologies as a function of $\bar{\phi}_{AB}$ and α. Here, we fixed $\chi_{BC}N_{AB} = -200.0$. The theoretical results are qualitatively consistent with the experimental observations. Specifically, at small α (which corresponds to the low molecular weight PS-*b*-PHS-L), we observe a transformation from lamellar to HEX cylindrical to BCC spherical microdomains with decreasing $\bar{\phi}_{AB}$. With increasing molecular weight of PS-*b*-PHS, we observe only a transformation from lamellar to HEX cylindrical microdomains with decreasing $\bar{\phi}_{AB}$. But, for very high molecular weight of PS-*b*-PHS, the lamellar microdomains remained.

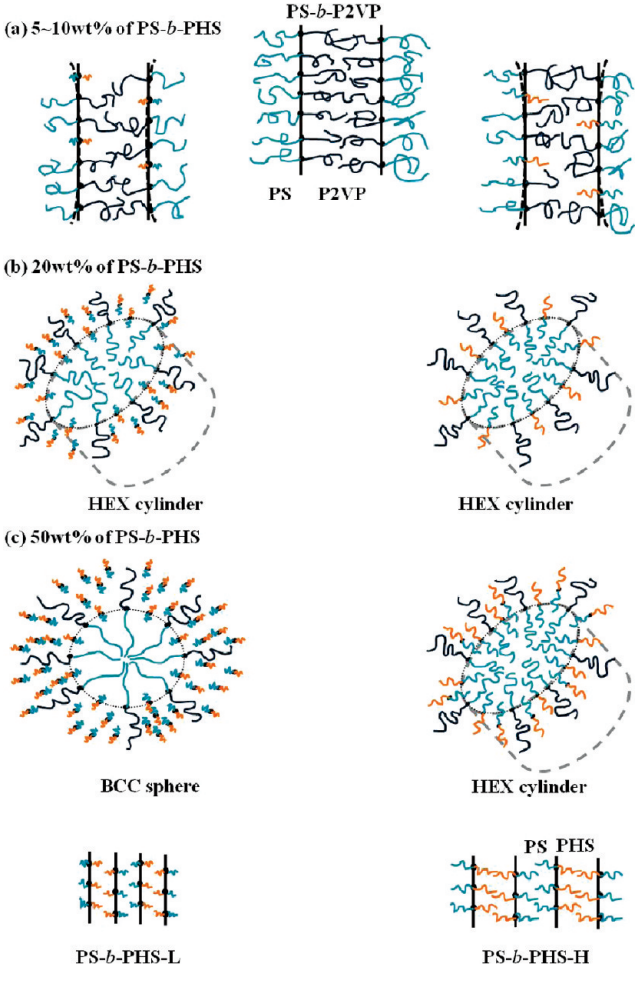

Figure 7. Scheme of the phase transformation of PS-*b*-P2VP/PS-*b*-PHS-L blend (left) and PS-*b*-P2VP/PS-*b*-PHS-H blend (right).

To understand the origins or mechanism of the phase transformations, in Figures 6a−c we display the equilibrium density profiles for the A, B, and C components as well as the distribution of the link points of the AB and AC in the HEX

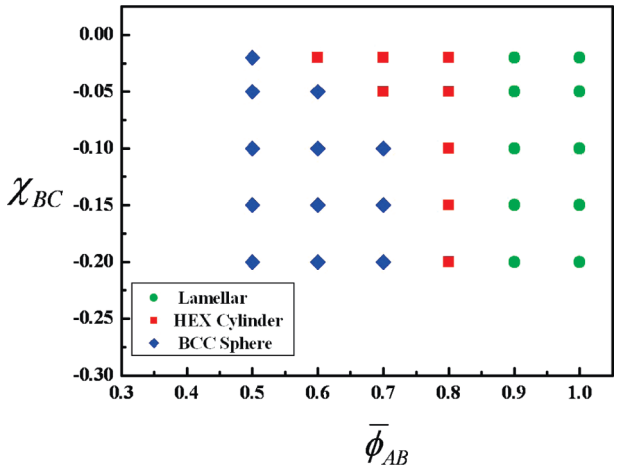

Figure 8. SCFT predictions of equilibrium phase diagram of AB/AC blend as a function of χ_{BC} at a given $\alpha = 0.125$.

cylindrical ($\bar{\phi}_{AB} = 0.8$) and BCC spherical microdomains ($\bar{\phi}_{AB} = 0.5$) at a given $\alpha = 0.125$.

In the HEX cylindrical and BCC spherical microdomains, a significant fraction of the AC links are located in the exterior B phase which is defined as the region to the right of the peak in the density distribution of the links of AB copolymers. Moreover, the fraction of AC copolymers dissolved in the B phase is larger at $\bar{\phi}_{AB} = 0.5$ compared to $\bar{\phi}_{AB} = 0.8$. It is also interesting to contrast the preceding results with the distributions observed for a larger AC chains ($\alpha = 0.2$) at $\bar{\phi}_{AB} = 0.5$ (the equilibrium morphology being a cylindrical phase). In the latter situation a significantly lower amount of AC links are present in the B phase (corresponding to the region $r/R \sim 1$ in the unit cell approximation).

Based on these results, the phase transformation on binary blends between PS-*b*-P2VP and PS-*b*-PHSs can be explained schematically as shown Figure 7. For PS-*b*-P2VP/PS-*b*-PHS-L blend and PS-*b*-P2VP/PS-*b*-PHS-H blend, at low content of PS-*b*-PHS, the PS-*b*-PHS would be expected to be located at the interface of PS-*b*-P2VP. Then, lamellar microdomains are expected to be maintained. But the PS-*b*-PHS chains in the interface could reduce the interfacial tension and the bending moduli of the interface, which might also contribute to a spontaneous curvature. With increasing overall amounts of PS-*b*-PHS, the amounts of PS-*b*-PHS dissolving in the P2VP phase increase due to the favorable interactions between PHS and P2VP and a gain of the translational entropy of the PS-*b*-PHS chains. These two effects lead to an increase in the "effective" volume fraction of the P2VP phase. Both increased the "effective" volume fraction of the P2VP phase and modified interfacial properties resulting in a transformation from lamellar to curved phases. However, for PS-*b*-PHS-H the amount dissolved in P2VP phase becomes smaller than PS-*b*-PHS-L at the same overall volume fraction $\bar{\phi}_{AB}$. The latter can be attributed to the reduced translational entropy gain of the AC chains as well as the more pronounced enthalpic cost arising from the unfavorable contacts between the A segments of the AC chain and the B segments in AB chains. In such a situation, the increase in the effective volume of the P2VP phase is decreased, and the phases in the PS-*b*-PHS-H are restricted to just the lamellar and HEX cylindrical microdomains in contrast to the lamellar, HEX cylindrical, and BCC spherical microdomains observed in PS-*b*-PHS-L.

Finally, the effect of the H-bonding interaction strength between PHS and P2VP on morphological transformations in the PS-*b*-P2VP/PS-*b*-PHS blend is shown in Figure 8. Here, we fixed $\alpha = 0.125$. With decreasing favorable B−C interactions (that is, χ_{BC} is decreased), the window corresponding to BCC spheres shrinks greatly. This is because of a reduction in the amount of PS-*b*-PHS dissolved in P2VP arising from less enthalpic gain.

In summary, we investigated the phase behavior of binary blends of block copolymers having hydrogen bonding. Binary blends with various blending composition between a higher molecular weight PS-*b*-P2VP and a lower molecular weight PS-*b*-PHS-L show the phase transformation from the lamellar, HEX cylindrical and BCC spherical microdomains, as increasing the amount of PS-*b*-PHS-L. However, for binary blends with PS-*b*-PHS-H, only HEX cylindrical microdomains are formed, not the BCC spherical microdomains even at a 50 wt % of PS-*b*-PHS-H. This is because PS-*b*-PHS-H could not easily swell into the P2VP microdomain due to the large enthalpic loss between PS/P2VP, unlike binary blends using PS-*b*-PHS-L. These results observed experimentally were consistent with predictions of the self-consistent mean-field theory.

■ ASSOCIATED CONTENT

Ⓢ Supporting Information. Temperature dependence of depolarized light intensity and the shear modulus (G') at a frequency (ω) = 0.1 rad/s for PS-*b*-PHS-L, FTIR spectra of binary blends with various blend compositions, details of the self-consistent field theory formalism. This material is available free of charge via the Internet at http://pubs.acs.org.

■ AUTHOR INFORMATION

Corresponding Author

*E-mail: jkkim@postech.ac.kr (J.K.K.); venkat@che.utexas.edu (V.G.).

■ ACKNOWLEDGMENT

This work was supported by the National Creative Research Initiative Program of the National Research Foundation of Korea (NRF). Small-angle X-ray scattering was performed at PLS beamline supported by POSCO and NRF. This work was partially supported by National Science Foundation under Awards 1005739 and 0730243 by a grant from Robert A. Welch Foundation (Grant F1599) and the US Army Research Office under Grant W911NF-10-1-0346. The authors acknowledge the Texas Advanced Computing Center (TACC) at The University of Texas at Austin for providing computing resources that have contributed to the research results reported within this paper.

■ REFERENCES

(1) Bates, F. S.; Fredrickson, G. H. *Annu. Rev. Phys. Chem.* **1990**, *41*, 525.
(2) Leibler, L. *Macromolecules* **1980**, *13*, 1602.
(3) Fredrickson, G. H.; Bates, F. S. *Annu. Rev. Mater. Sci.* **1996**, *26*, 501.
(4) Hashimoto, T. In *Thermoplastic Elastomer*, 2nd ed.; Holden, G., Legge, N. R., Quirk, R., Schroeder, H. E., Eds.; Hanser: Munich, 1996; Chapter 15A.
(5) Hamley, I. W. *The Physics of Block Copolymers*; Oxford University Press: New York, 1998.
(6) Helfand, E.; Wasserman, Z. R. In *Developments in Block Copolymer*; Goodman, I., Ed.; Applied Science: New York, 1982.

(7) Han, C. D. *Rheology and Processing of Polymeric Materials*; Oxford University Press: Oxford, 2007; Vol. 1.
(8) Park, C.; Yoon, J.; Thomas, E. L. *Polymer* **2003**, *44*, 6725.
(9) Kim, J. K.; Han, C. D. *Adv. Polym. Sci.* **2010**, *231*, 77.
(10) Kim, J. K.; Yang, S. Y.; Lee, Y. M.; Kim, Y. S. *Prog. Polym. Sci.* **2010**, *35*, 1325.
(11) Kim, J. K.; Lee, J. I.; Lee, D. H. *Macromol. Res.* **2008**, *16*, 267.
(12) Han, C. D.; Baek, D. M.; Kim, J. K.; Ogawa, T.; Sakamoto, N.; Hashimoto, T. *Macromolecules* **1995**, *28*, 5043.
(13) Ryu, D. Y.; Jeong, U.; Kim, J. K.; Russell, T. P. *Nature Mater.* **2002**, *1*, 114.
(14) Ryu, D. Y.; Lee, D. J.; Kim, J. K.; Lavery, K. A.; Russell, T. P.; Han, Y. S.; Seong, B. S.; Lee, C. H.; Thiyagarajan, P. *Phys. Rev. Lett.* **2003**, *90*, 235501.
(15) Jo, A. R.; Joo, W. C.; Jin, W. H.; Nam, H. J.; Kim, J. K. *Nature Nanotechnol.* **2009**, *4*, 727.
(16) Semenov, A. N. *Sov. Phys. JETP* **1985**, *61*, 733.
(17) Matsen, M. W.; Bates, F. S. *Macromolecules* **1996**, *29*, 1091.
(18) Hasegawa, H.; Tanaka, H.; Yamasaki, K.; Hashimoto, T. *Macromolecules* **1987**, *20*, 1651.
(19) Khandpur, A. K.; Foerster, S.; Bates, F. S.; Hamley, I. W.; Ryan, A. J.; Bras, W.; Almdal, K.; Mortensen, K. *Macromolecules* **1995**, *28*, 8796.
(20) Han, C. D.; Baek, D. M.; Kim, J. K.; Ogawa, T.; Sakamoto, N.; Hashimoto, T. *Macromolecules* **1995**, *28*, 5043.
(21) Sakurai, S.; Umeda, H.; Furukawa, C.; Irie, H.; Nomura, S.; Lee, H. H.; Kim., J. K. *J. Chem. Phys.* **1998**, *108*, 4333.
(22) Sakurai, S.; Irie, H.; Umeda, H.; Nomura, S.; Lee, H. H.; Kim., J. K. *Macromolecules* **1998**, *31*, 336.
(23) Yamaguchi, D.; Hashimoto, T.; Han, C. D.; Baek, D. M.; Kim, Lee, H. H.; Kim, J. K.; Shi, A.-C. *Macromolecules* **1997**, *30*, 5832.
(24) Shi, A.-C.; Noolandi, J. *Macromolecules* **1994**, *27*, 2936.
(25) Shi, A.-C.; Noolandi, J.; Hoffman, H. *Macromolecules* **1994**, *27*, 6661.
(26) Shi, A.-C.; Noolandi, J. *Macromolecules* **1995**, *28*, 3103.
(27) Lin, E. K.; Gast, A. P.; Shi, A.-C.; Noolandi, J.; Smith, S. D. *Macromolecules* **1996**, *29*, 5920.
(28) Wu, Z.; Li, B.; Jin, Q.; Ding, D.; Shi, A.-C. *Macromolecules* **2011**, *44*, 1680.
(29) Court, F.; Hashimoto, T. *Macromolecules* **2001**, *34*, 2536.
(30) Court, F.; Hashimoto, T. *Macromolecules* **2002**, *35*, 2566.
(31) Court, F.; Yamaguchi, D.; Hashimoto, T. *Macromolecules* **2006**, *39*, 2596.
(32) Court, F.; Yamaguchi, D.; Hashimoto, T. *Macromolecules* **2008**, *41*, 4828.
(33) Yamaguchi, D.; Hashimoto, T. *Macromolecules* **2001**, *34*, 6495.
(34) Yamaguchi, D.; Hashimoto, T. *Macromolecules* **2001**, *34*, 6506.
(35) Kimishima, K.; Jinnai, H.; Hashimoto, T. *Macromolecules* **1999**, *32*, 2585.
(36) Vaidya, N. Y.; Han, C. D. *Macromolecules* **2000**, *33*, 3009.
(37) Mao, H.; Hillmyer, M. A. *Macromolecules* **2008**, *209*, 1647.
(38) Asari, T.; Matsuo, S.; Takano, A.; Matsushita, Y. *Macromolecules* **2005**, *38*, 8811.
(39) Asari, T.; Arai, S.; Takano, A.; Matsushita, Y. *Macromolecules* **2006**, *39*, 2232.
(40) Chen, S.-C.; Kuo, S.-W.; Jeng, U.-S.; Su, C.-J.; Chang, F.-C. *Macromolecules* **2010**, *43*, 1083.
(41) Fredrickson, G. H. *The Equilibrium Theory of Inhomogeneous Polymers*; Oxford University Press: New York, 2006.
(42) Fredrickson, G. H.; Ganesan, V.; Drolet, F. *Macromolecules* **2002**, *35*, 16.
(43) Matsen, M. W. *Macromolecules* **2003**, *36*, 9647.
(44) Matsen, M. W.; Whitmore, M. D. *J. Chem. Phys.* **1996**, *105*, 9698.
(45) Vavasour, J. D.; Whitmore, M. D. *Macromolecules* **1992**, *25*, 5477.
(46) Wu, Z.; Li, B.; Jin, Q.; Ding, D.; Shi, A.-C. *J. Phys. Chem. B* **2010**, *114*, 15789.
(47) Li, M.; Douki, K.; Goto, K.; Li, X.; Coenjarts, C.; Smilgies, D. M.; Ober, C. K. *Chem. Mater.* **2004**, *16*, 3800.
(48) Bolze, J.; Kim, J.; Huang, J. Y.; Rha, S.; Youn, H. S.; Lee, B.; Shin, T. J.; Ree, M. *Macromol. Res.* **2002**, *10*, 2.
(49) Zhu, K. J.; Chen, S. F.; Ho, T.; Pearce, E. M.; Kwei, T. K. *Macromolecules* **1990**, *23*, 150.
(50) Alberda van Ekenstein, G. O. R.; Mayboom, R.; ten Brinke, G.; Ikkala, O. *Macromolecules* **2000**, *33*, 3752.
(51) Zha, W.; Han, C. D.; Lee, D. H.; Han, S. H.; Kim, J. K.; Kang, J. H.; Park, C. *Macromolecules* **2007**, *40*, 2109.
(52) Han, S. H.; Lee, D. H.; Kim, J. K. *Macromolecules* **2007**, *40*, 7416.
(53) Dobrosielska, K.; Wakao, S.; Takano, A.; Matsushita, Y. *Macromolecules* **2008**, *41*, 7695.
(54) Dobrosielska, K.; Wakao, S.; Suzuki, J.; Noda, K.; Takano, A.; Matsushita, Y. *Macromolecules* **2009**, *42*, 7098.
(55) Lefevre, N.; Daoulas, K. C.; Muller, M.; Gohy, J.-F.; Fustin, C.-A. *Macromolecules* **2010**, *43*, 7734.